

# A Phosphonated Poly(ethylenedioxythiophene) Derivative with Low Oxidation Potential for Energy-Efficient Bioelectronic Devices

Jonathan Hopkins, Kristina Fidanovski, Lorenzo Travaglini, Daniel Ta, James Hook, Pawel Wagner, Klaudia Wagner, Antonio Lauto, Claudio Cazorla, David Officer, and Damia Mawad\*



Cite This: *Chem. Mater.* 2022, 34, 140–151



Read Online

ACCESS |



Metrics & More

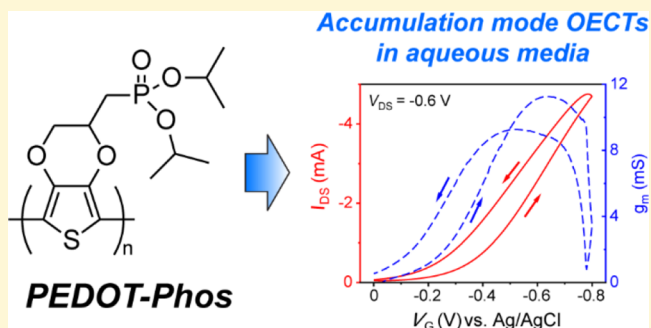


Article Recommendations



Supporting Information

**ABSTRACT:** Organic electrochemical transistors (OECTs) for bioelectronic applications require the design of conjugated polymers that are stable in aqueous environments and afford high energy efficiency and good performance in OECTs. Polymers based on poly(ethylenedioxythiophene) (PEDOT) are promising in this area due to their low oxidation potential and reversible redox, but they often require cross-linking to prevent dissolution and yield OECTs operating in the less efficient depletion mode. In this work, a new conjugated polymer PEDOT-Phos is presented, which combines a conjugated poly(ethylenedioxythiophene) (PEDOT) backbone with alkyl-protected phosphonate groups. PEDOT-Phos exhibits a low oxidation onset potential ( $-0.157$  V vs Ag/AgCl) and its nanoporous morphology affords it a high volumetric capacitance ( $282 \pm 62$  F cm $^{-3}$ ). Without any cross-linking, additives, or post-treatment, PEDOT-Phos can be used in aqueous OECTs with efficient accumulation mode operation, long-term stability when immersed in aqueous media, low threshold voltages ( $-0.161 \pm 0.005$  V), good transconductances ( $9.3 \pm 1.8$  mS), and ON/OFF current ratios ( $618 \pm 54$ ) comparable to other PEDOT-based materials in OECTs. These results highlight the great promise of PEDOT-Phos as a stand-alone channel material for energy-efficient, bioelectronic devices.



## 1. INTRODUCTION

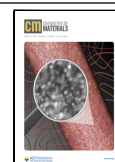
Organic electrochemical transistors (OECTs) transform small fluctuations in gate voltage  $V_G$  into large changes in the source-drain current  $I_{DS}$  via an organic semiconducting channel material with mixed ionic-electronic conductivity, usually a conjugated polymer (CP).<sup>1</sup> Their efficient amplification of the incoming signal gives OECTs great utility in biological applications, where they have been used in the sensitive detection of biomolecules<sup>2–4</sup> and in monitoring of low-intensity ionic signals in biological cells when interfaced with living tissues.<sup>3,5</sup> In these applications, OECTs must operate with high energy efficiency and at low threshold voltages to prevent additional reactions, which may interfere with biological cell signals.<sup>6</sup> The CP used as the channel material should permit the penetration of ions from the aqueous electrolyte and store charge during device operation, corresponding to a high volumetric capacitance,  $C^*$ .<sup>7</sup> The channel material should also be both insoluble and electroactive in physiological media. These requirements have driven the recent design of organic semiconductors for use in bioelectronics<sup>8,9</sup> and also formed the basis for the present work. Our aim was to design and characterize a new, CP-based channel material according to the above criteria for use in aqueous, accumulation mode OECTs.

The channel material in an OECT is reversibly doped and de-doped as the gate potential changes, and this process is accompanied by ions diffusing into and out of the channel.<sup>10</sup> Since the entire channel volume is accessible to ions and thus involved in signal transduction, OECTs exhibit large signal amplification compared to organic field-effect transistors (OFETs) that rely only on charge accumulation at the channel surface.<sup>1</sup> The efficiency of this amplification is expressed as the device transconductance, defined as  $g_m = \partial I_{DS} / \partial V_G$ .<sup>1,5</sup> The energy efficiency of OECTs can also be improved by selecting a channel material that facilitates device operation in accumulation mode rather than depletion mode. In accumulation mode, the channel material is not initially doped and does not allow current to pass between the source and drain, and the device is in the OFF state. When a  $V_G$  is applied, ions diffuse into the channel to dope it, allowing current to pass through the channel, and the device switches ON. In contrast, in depletion mode operation, the channel is initially doped and

Received: August 25, 2021

Revised: December 16, 2021

Published: December 28, 2021



permits the source-drain current to pass through. In this case, energy is required to constantly apply a large gate bias to keep the device OFF, which lowers the device's energy efficiency.<sup>11</sup>

CPs are an ideal class of material for the channel due to their biocompatibility and versatile chemical functionalization, which have led to wide-ranging applications including electrochemical biosensors,<sup>12</sup> cell signal monitoring,<sup>13</sup> and optoelectronic cell stimulation,<sup>14</sup> as well as OECTs.<sup>7</sup> Recent material designs for accumulation mode OECTs have especially focused on functionalized derivatives of poly(thiophene), including water-processible derivatives bearing sulfonate<sup>6,15</sup> and carboxylate<sup>16</sup> pendant groups. Derivatives with ethylene glycol side chains, such as poly(2-(3,3'-bis(2-(2-(2-methoxyethoxy)ethoxy)ethoxy)-[2,2'-bithiophen]-5-yl)-thieno[3,2-*b*]thiophene) (p(g2T-TT)), have also been used in accumulation mode OECTs with good performances in aqueous media.<sup>9</sup> However, a potential limitation of poly(thiophene) derivatives is their high oxidation potentials, which for p(g2T-TT), manifests in its reversible doping at +0.5 V vs Ag/AgCl in *in situ* spectroelectrochemistry.<sup>17</sup> On the other hand, CPs based on poly(ethylenedioxythiophene) (PEDOT) are appealing since the PEDOT backbone affords a low oxidation potential and relatively small band gap energy,<sup>18</sup> as well as good redox stability.<sup>19</sup> Consequently, the water-processible dispersion poly(ethylenedioxythiophene):poly(styrene sulfonate) (PEDOT:PSS) has become a "gold-standard" material for OECTs.<sup>20,21</sup> In addition to PEDOT:PSS, the main PEDOT-based alternative used in OECTs is the conjugated polyelectrolyte poly(sodium 4-((2,3-dihydrothieno[3,4-*b*]-[1,4]dioxin-2-yl)methoxy)butane-1-sulfonate) (PEDOT-S).<sup>22,23</sup> However, both these materials yield OECTs that operate in the less-efficient depletion mode. To achieve accumulation mode devices, further treatments are required such as overoxidation of PEDOT:PSS<sup>24</sup> or blending it with other semiconducting polymers such as poly(tetrabutylammonium 6-(thiophene-3-yl)hexane-1-sulfonate) (PTHS).<sup>22</sup> These CPs are also water-processible and must undergo additional post-treatment or cross-linking to ensure their stability in aqueous OECTs; cross-linking in particular decreases ionic mobility and hinders the crucial diffusion of ions in the channel.<sup>8</sup> Given the lack of other PEDOT derivatives used in OECTs, there remains a clear opportunity to develop PEDOT-based channel materials for aqueous OECTs that operate at mild, biofriendly potentials and do not require additives or post-treatment.

A potential means of achieving this goal lies in CPs bearing pendant phosphonate functionalities. The prevalence of phosphonate groups in biological systems enables a bio-inspired design approach to develop electroactive materials that can detect biomolecules or be interfaced with living tissues in bioelectronics.<sup>25</sup> Furthermore, CPs with alkyl-protected phosphonate groups are processible in organic solvents and so can be used to fabricate water-stable, electroactive films without requiring post-treatment. They have been used as emission and electron-injection layers in OLEDs;<sup>26,27</sup> however, they remain underdeveloped compared to CPs bearing sulfonate and carboxylate groups. They have not yet been utilized in OECTs, and the applications of phosphonated CPs are dominated by derivatives of poly(fluorene), leaving many chemical designs for phosphonated CPs unexplored. In particular, phosphonated CPs that utilize the low oxidation

potential and redox stability of the PEDOT backbone have not yet been reported.

Therefore, in this work, we present the synthesis and detailed characterization of a new PEDOT derivative bearing isopropyl-protected phosphonate pendant groups (PEDOT-Phos). Each phosphonate group is separated from the PEDOT backbone by a single methylene spacer. We synthesized the phosphonated monomer EDOT-Phos as the diisopropyl-phosphonate ester then performed chemical oxidative polymerization to yield the alkyl-protected polymer PEDOT-Phos. We then characterized the polymer's chemical structure as well as its optical, morphological, and electronic properties. PEDOT-Phos is organic-processable and undergoes reversible electrochemistry at low potentials in aqueous electrolytes. Importantly, we also demonstrated the use of PEDOT-Phos without any post-treatment in accumulation mode OECTs operating in aqueous NaCl solution.

## 2. EXPERIMENTAL SECTION

**2.1. Materials.** (2,3-Dihydrothieno[3,4-*b*][1,4]dioxin-2-yl)-methanol (EDOT-OH, 95%) was purchased from Molekula Ltd., U.K. *p*-Toluenesulfonyl chloride (TosCl) and 4-dimethylaminopyridine (DMAP) were purchased from Arcos Organics and used as received. Deuterated chloroform (CDCl<sub>3</sub>) was obtained from Cambridge Isotope Laboratories. Sodium hydroxide pellets (NaOH) and sodium hydrogen carbonate (NaHCO<sub>3</sub>) were obtained from Univar. Toluene (ChemSupply) was dried over molecular sieve absorbent beads (3 Å, 8–12 mesh, Sigma-Aldrich) and stored under nitrogen. All other chemicals were obtained from Sigma-Aldrich or ChemSupply and used as received. For column chromatography, chromatographic silica media LC60A (40–63 micron) and thin-layer chromatographic silica gel 60 F254 plates (Merck) with a dimension of 20 × 20 cm and no fluorescence indicator were purchased from Sigma-Aldrich, and acid-washed sand (grain size of ~300–350 μm) was obtained from ChemSupply.

**2.2. Synthesis of (2,3-Dihydrothieno[3,4-*b*][1,4]dioxin-2-yl)methyl 4-Methylbenzenesulfonate (EDOT-Tos).** EDOT-OH (505.6 mg, 2.90 mmol) was dissolved in anhydrous chloroform (10.0 mL) in a round-bottom flask. TosCl (1106.0 mg, 5.80 mmol, 2 mol equiv), triethylamine (TEA, 1.13 mL, 8.13 mmol, 2.8 mol equiv), and DMAP (72.4 mg, 0.59 mmol, 0.2 mol equiv) were sequentially added. The reaction mixture was stirred for 4 h at room temperature under nitrogen, with the reaction progress monitored using thin-layer chromatography (TLC). To quench the reaction, a 10 v/v % aqueous solution of sulfuric acid (H<sub>2</sub>SO<sub>4</sub>, 25 mL) and saturated aqueous NaHCO<sub>3</sub> solution (50 mL) were added dropwise. The organic layer was washed three times with saturated NaHCO<sub>3</sub> solution and dried over anhydrous magnesium sulfate (MgSO<sub>4</sub>). After rotary evaporation, the product EDOT-Tos (925 mg, 98%) was obtained and analyzed by <sup>1</sup>H NMR (400 MHz, CDCl<sub>3</sub>) δ (ppm): 7.80 (d, 2H, tosyl ArH), 7.36 (d, 2H, tosyl ArH), 6.32 & 6.26 (dd, 2H, thiophene CH), 4.36 (m, 1H, ethylenedioxy CH), 4.22 (m, 2H, methylene CH<sub>2</sub>), 4.18 (dd, 1H, ethylenedioxy CH<sub>2</sub>), 4.03 (dd, 1H, ethylenedioxy CH<sub>2</sub>), 2.46 (s, 3H, tosyl CH<sub>3</sub>). <sup>13</sup>C NMR (100 MHz, CDCl<sub>3</sub>) δ: 145.3 (tosyl aromatic SO<sub>2</sub>-C-(CH<sub>2</sub>)), 140.9 & 140.4 (thiophene β-C), 132.4 (tosyl aromatic (CH<sub>2</sub>-C-CH<sub>3</sub>)), 130.0 (tosyl aromatic (C-H)<sub>2</sub>CCH<sub>3</sub>), 128.1 (tosyl aromatic SO<sub>2</sub>C-(C-H)<sub>2</sub>), 100.2 (thiophene α-C), 70.8 (ethylenedioxy CH), 66.9 (methylene CH<sub>2</sub>), 65.0 (ethylenedioxy CH<sub>2</sub>), 21.7 (tosyl CH<sub>3</sub>).

**2.3. Synthesis of 2-(Iodomethyl)-2,3-dihydrothieno[3,4-*b*]-[1,4]dioxine (EDOT-I).** EDOT-Tos (872.2 mg, 2.67 mmol) was dissolved in acetone (33.5 mL) under nitrogen. Sodium iodide (NaI, 7.94 g, 53.4 mmol, 20 mol equiv) was added and the reaction mixture was refluxed at 60 °C for 18 h, with the reaction progress monitored using TLC. Solvent was removed by rotary evaporation and the product was purified using flash column chromatography with ethyl acetate (EtOAc):TEA:*n*-hexane (29:1:70 v/v %) as eluent, yielding EDOT-I (567 mg, 75%). <sup>1</sup>H NMR (400 MHz, CDCl<sub>3</sub>) δ: (ppm) 6.36

(dd, 2H, thiophene CH), 4.31 (dd, 1H, ethylenedioxy CH<sub>2</sub>), 4.26 (m, 1H, ethylenedioxy CH), 4.15 (dd, 1H, ethylenedioxy CH), 3.33 (m, 2H, methylene CH<sub>2</sub>). <sup>13</sup>C NMR (100 MHz, CDCl<sub>3</sub>) δ: 141.1 & 140.8 (thiophene β-C), 100.1 & 100.0 (thiophene α-C), 72.9 (ethylenedioxy CH), 67.3 (ethylenedioxy CH<sub>2</sub>), 0.7 (methylene CH<sub>2</sub>).

**2.4. Synthesis of Diisopropyl ((2,3-Dihydrothieno[3,4-*b*]-[1,4]dioxin-2-yl)methyl)phosphonate (EDOT-Phos).** EDOT-I (536.1 mg, 1.90 mmol) was dissolved in anhydrous toluene (5.0 mL) in a dry round-bottom flask under a nitrogen atmosphere. Triisopropylphosphite (P(Oi-Pr)<sub>3</sub>, 0.99 mL, 3.80 mmol, 2 mol equiv) was added dropwise to the reaction mixture, and the mixture was heated at 120 °C. At 8, 24, and 32 h, the reaction mixture was briefly cooled to room temperature and additional P(Oi-Pr)<sub>3</sub> (0.49 mL, 1.90 mmol, 1 mol equiv) was added dropwise. After 48 h, the reaction mixture was cooled and toluene was removed by rotary evaporation. The crude product was purified using flash column chromatography with EtOAc:TEA:*n*-hexane (29:1:70 v/v%) initially, and then EtOAc:TEA (99:1 v/v%) was used as eluent. The product EDOT-Phos (308.8 mg, 51%) was obtained and analyzed by <sup>1</sup>H NMR (400 MHz, CDCl<sub>3</sub>) δ: 6.32 (dd, 2H, thiophene CH), 4.75 (m, 2H, *J*<sub>HP</sub> = 7.8 Hz, isopropyl CH), 4.49 (m, 1H, *J*<sub>HP</sub> = 9.4 Hz, ethylenedioxy CH), 4.35 (dd, 1H, ethylenedioxy CH<sub>2</sub>), 3.97 (dd, 1H, ethylenedioxy CH<sub>2</sub>), 2.20 (dd, 1H, *J*<sub>HP</sub> = 20.0 Hz, methylene CH<sub>2</sub>), 2.06 (dd, 1H, *J*<sub>HP</sub> = 15.3 Hz, methylene CH<sub>2</sub>), 1.34 (dd, 12H, isopropyl CH<sub>3</sub>). <sup>13</sup>C NMR (100 MHz, CDCl<sub>3</sub>) δ: 141.2 & 141.2 (thiophene β-C), 99.9 & 99.7 (thiophene α-C), 70.8 (isopropyl CH), 69.4 (ethylenedioxy CH), 68.0 & 68.0 (ethylenedioxy CH<sub>2</sub>), 30.3 & 28.9 (*J*<sub>CP</sub> = 143 Hz, methylene CH<sub>2</sub>), 24.0 (isopropyl CH<sub>3</sub>). <sup>31</sup>P NMR (162 MHz, CDCl<sub>3</sub>) δ: 23.3 (phosphonate P).

**2.5. Synthesis of PEDOT-Phos.** Powdered iron(III) chloride (FeCl<sub>3</sub>, 649.1 mg, 4.00 mmol) was dispersed in anhydrous chloroform (14.0 mL) under nitrogen. Separately, EDOT-Phos (308.8 mg, 0.964 mmol) was dissolved in anhydrous chloroform (2.5 mL) and this solution was added dropwise to the reaction flask. The mixture was stirred at ambient temperature for 24 h. The mixture was poured into an excess of methanol and centrifuged at 7000 rpm for 5 min, and the supernatant was decanted off. The remaining solid product was washed and centrifuged down (four times with methanol and twice with deionized water) then freeze-dried, yielding a flaky, black, oxidized polymer powder (oxidized PEDOT-Phos, 192 mg, 30%). To reduce the oxidized polymer, oxidized PEDOT-Phos (24.0 mg) was dispersed in CHCl<sub>3</sub> (4 mL) in a glass vial, and hydrazine monohydrate (4 drops) was added. The mixture was stirred overnight at room temperature then decanted into a separatory funnel and washed three times with deionized water. The purple, organic layer was collected, and solvent was removed by rotary evaporation. The product was obtained as a flaky, dark purple solid (PEDOT-Phos) that was resolubilized as required. <sup>31</sup>P NMR (162 MHz, CDCl<sub>3</sub>) δ: 22.9.

**2.6. Fabrication of Polymer Films.** Polymer solutions were prepared by dissolving PEDOT-Phos in CHCl<sub>3</sub> (5.0 mg/mL) at room temperature. Before fabricating the film, glass slides and indium tin oxide (ITO)-coated glass substrates were cleaned by immersion in basic piranha solution at 60 °C for 15 min, then rinsed with deionized water and acetone, and dried under a flow of nitrogen gas. Films were then produced by drop-casting the solutions onto the substrates and leaving them to dry at room temperature. For atomic force microscopy (AFM), cyclic voltammetry (CV), X-ray photoelectron spectroscopy (XPS), and photoluminescence (PL) spectroscopy, the polymer solution (20 μL) was drop-casted onto an area of 8 × 5 mm for AFM, CV, and EIS or 8 × 8 mm for XPS and PL. For *in situ* UV-vis-NIR spectroelectrochemistry, the solution (40 μL) was drop-casted onto an area of 8 × 45 mm in dimension. These film areas were controlled by securing a thin strip of tape to the substrate at the edge of the required area before drop-casting. For OECT measurements and electrochemical impedance spectroscopy (EIS), the solution (10 μL) was drop-casted onto an interdigitated microelectrode (IDME) purchased from Micrux Technologies (ED-IDE1-Au) with channel width *W* = 50 cm and channel length *L* = 10 μm. A Dektak IIA

profilometer with tilt correction was used to measure the thickness of the dry film, *d* = 579 ± 73 nm.

**2.7. Structural Characterization.** Solution nuclear magnetic resonance (NMR) spectroscopy was performed using a Bruker Avance III 400 spectrometer (400.14 MHz, <sup>1</sup>H; 100.62 MHz, <sup>13</sup>C; 161.97 MHz, <sup>31</sup>P) with a 5 mm BBO probe. Samples were analyzed at 298 K in CDCl<sub>3</sub> filtered through anhydrous solid K<sub>2</sub>CO<sub>3</sub> directly before use. All chemical shifts are stated in ppm (δ) relative to tetramethylsilane (δ = 0), referenced to the chemical shifts of residual solvent resonances (<sup>1</sup>H, δ<sub>H</sub> = 7.26 and <sup>13</sup>C, δ<sub>C</sub> = 77.0). Coupling constants (*J*) are reported in hertz, and multiplicities are denoted as singlet (s), doublet (d), triplet (t), quartet (q), or multiplet (m). The <sup>31</sup>P spectra were calibrated to H<sub>3</sub>PO<sub>4</sub> (85%) (δ<sub>P</sub> = 0). The NMR spectra were processed using Bruker TopSpin 4.1.0 software.

Gel permeation chromatography (GPC) was performed using an LC20A HPLC system (Shimadzu). A Styragel HT4 column (Waters, WAT044511) was used with a particle size of 10 μm, inner diameter of 7.8 mm, and length of 300 mm. Detection was performed using a refractive index detector (RID-10A) and a photodiode array detector (SPD-M20A). The sample was eluted at 30 °C in DMF with a flow rate of 1 mL min<sup>-1</sup>. Calibration was performed to polystyrene standards ranging from 1350 to 500,800 Da. The chromatograms were processed using Shimadzu LC solution software.

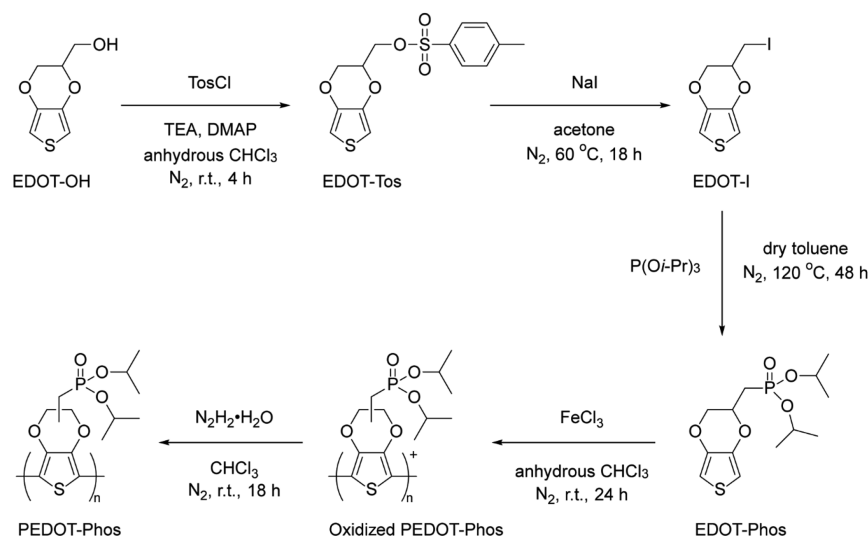
Fourier transform infrared spectroscopy (FTIR) of drop-casted films on glass/ITO substrates was conducted using a Spectrum Two FTIR spectrometer (Perkin Elmer) operating in attenuated total reflectance (ATR) mode. The spectra were obtained over the wavenumber range of 4000–450 cm<sup>-1</sup> using eight accumulations and a wavenumber resolution of 2 cm<sup>-1</sup>. Raman spectroscopy of films on glass/ITO substrates was conducted at a wavelength of 532 nm using a Raman microscope and spectrometer (inVia, Renishaw) calibrated against an internal silicon standard. The spectra were acquired over the wavenumber range of 3200–60 cm<sup>-1</sup> using four accumulations of 10 s each.

XPS was performed using a Thermo ESCALAB 250 Xi X-ray photoelectron spectrometer (Thermo Scientific, U.K.). Samples were analyzed under high vacuum (better than 2 × 10<sup>-9</sup> mbar) with monochromated Al Kα (1486.68 eV) as the X-ray source from an anode operating at 120 W and a spot size of 500 μm. The spectrometer was calibrated using the Au 4f<sub>7/2</sub> = 83.96 eV, Ag 3d<sub>5/2</sub> = 368.21 eV, and Cu 2p<sub>3/2</sub> = 932.62 eV lines. The tube voltage was 13.8 kV, the tube current was 8.7 mA, and the pass energy was 100 eV for survey scans and 20 eV for scans of individual regions. The binding energies were referenced to the C 1s adventitious hydrocarbon peak at 284.8 eV. The peaks were deconvoluted and fitted to a mixed Gaussian–Lorentzian model using Avantage software, with the full width half-maxima (FWHM) constrained to 1.0 eV for P and S and 1.2 eV for C.

**2.8. Optical, Electrochemical, and Theoretical Characterizations.** The absorption spectra of polymer solutions and films were recorded using a UV-vis-NIR spectrometer (Lambda 1050, PerkinElmer). Photoluminescence spectroscopy of PEDOT-Phos films was conducted at a wavelength of 325 nm using a Raman microscope and spectrometer (inVia, Renishaw). The spectra were acquired over the wavelength range of 1000–350 nm with two accumulations. Cosmic rays were removed from the spectra in post-processing.

Electrochemical characterization was performed in either sodium chloride (NaCl, 0.1 M in deionized water) or tetrabutylammonium tetrafluoroborate (TBABF<sub>4</sub>, 0.1 M in acetonitrile). The aqueous reference electrode was a Ag/AgCl aqueous reference electrode in 1 M potassium chloride (CHI Instruments). The organic reference electrode was a Ag/Ag<sup>+</sup> non-aqueous reference electrode in 0.1 M TBABF<sub>4</sub> and 0.01 M AgNO<sub>3</sub> (CHI Instruments). A Pt coil was used as the counter electrode. CV and EIS were performed using a potentiostat (Vertex, IVIUM). Cyclic voltammograms were obtained for various scan rates, potential ranges, and numbers of cycles. *In situ* UV-vis-NIR spectroelectrochemistry and double-step spectrochromamperometry of PEDOT-Phos/ITO films were performed using a spectrophotometer (UV-1800, Shimadzu) to acquire the absorbance

## Scheme 1. Synthesis of Monomers and the Polymer PEDOT-Phos



spectra and a potentiostat (eDAQ) controlled by EChem software to apply potential. Before obtaining spectroelectrochemistry data, each film was initially relaxed with six cycles of CV between  $-0.3$  and  $+1.1$  V vs Ag wire ( $-0.64$  to  $+0.76$  V vs Ag/AgCl). For spectrochromoamperometry, from 10 s onward, the potential was switched between  $+0.8$  and  $-0.6$  V (both vs Ag/AgCl), holding each potential for 20 s, and the absorbance at 560 nm was recorded as a function of time. The oxidation onset potential  $E_{ox}$  was obtained from the cyclic voltammograms, and the HOMO energy level and ionization potential (IP) were estimated from  $E_{ox}$  using the following equation:  $IP = -E_{HOMO} = (E_{ox} - E_{Fc,1/2} + 0.624 + 4.44)$  eV, where  $+0.624$  V is the ferrocene/ferrocenium ( $Fc/Fc^+$ ) potential in acetonitrile versus SHE<sup>28</sup> and  $+4.44$  V is the absolute potential of the standard hydrogen electrode.  $E_{Fc,1/2}$  is the half-wave potential of  $Fc/Fc^+$  in acetonitrile, taken as the average of the oxidation and reduction peak potentials; we measured this half potential to be  $+0.168$  V vs Ag/Ag<sup>+</sup>.

First-principles calculations based on density functional theory (DFT) were performed using the Katana HPC cluster<sup>29</sup> to simulate the electrical band gap, band structure, and ionization potential of PEDOT-Phos for comparison with experimental data. We conducted DFT calculations using the Vienna Ab Initio Simulation Package (VASP)<sup>30</sup> with projector-augmented wave potentials and an energy cutoff of 750 eV. The generalized gradient approximation to the exchange-correlation energy was that developed by Perdew *et al.*,<sup>31</sup> and dispersion interactions were handled using the zero-damping DFT-D3 method of Grimme *et al.*<sup>32</sup> The following electronic states were considered as valence: C 2s and 2p, S 3s and 3p, O 2s and 2p, H 1s, and P 3s and 3p. The two cases tested were an isolated PEDOT-Phos chain (containing 78 atoms), with two repeat units in an orthorhombic unit cell (Figure S16A), and a PEDOT-Phos crystalline solid (containing 156 atoms), comprising two stacked chains with two repeat units each, in a monoclinic unit cell (Figure S16B). In both cases, the polymer backbone repeated along the *c*-direction with  $\pi$ -stacking in the *b*-direction. Periodic boundary conditions were applied in all three directions. For the isolated chain, a vacuum region of roughly 30 Å was added to the simulation cell in the *a*- and *b*-directions to eliminate interchain interactions. The initial geometry was relaxed to a final force tolerance of  $0.01$  eV Å<sup>-1</sup>, with an energy tolerance of  $0.1$   $\mu$ eV per atom for each ionic step. A Monkhorst–Pack *k*-point grid of  $1 \times 1 \times 2$  (isolated chain) or  $2 \times 6 \times 6$  (crystalline solid) was used. Self-consistent charge densities were obtained and used to calculate the band structure *via* a non-self-consistent calculation with 25 *k*-points between various high-symmetry points in the unit cell. The effective masses of charge carriers were calculated by applying a parabolic fit to the valence and conduction band energies plotted as a function of *k*-point distance. We extracted the vacuum energy ( $E_{vac}$ ) by calculating the local potential along one of

the vacuum directions for the isolated molecule. From this, we estimated the HOMO and LUMO energy levels ( $E_{HOMO}$  and  $E_{LUMO}$ ) and ionization potential (IP) using the following equations:  $IP = -E_{HOMO} = E_{vac} - E_F + 2E_g$  and  $E_{LUMO} = E_{HOMO} + 2E_g$ , where  $E_F$  and  $E_g$  are the Fermi level and theoretical electronic band gap, respectively. The theoretical  $E_g$  was multiplied by a factor of two to compensate for the DFT results underestimating the band gap, as has been previously observed for PEDOT<sup>33</sup> and other semiconductors.<sup>34</sup>

The surface topography of the PEDOT-Phos films before and after CV was characterized using an atomic force microscope (NanoWizard II; JPK Instruments AG, Berlin, Germany). The microscope was operated in intermittent-contact mode, both in air and liquid, for imaging. Phosphate-buffered saline (PBS) solution was used during aqueous imaging as the liquid medium. Images were taken with a nominal spring constant of  $32$  Nm<sup>-1</sup> and a resonant frequency of 315 kHz using silicon cantilevers (Type ACT; AppNano, Mountain View, CA, USA). With a pixel resolution of  $512 \times 512$ , the scan rate was set to 1 Hz. Three separate  $50 \times 50$   $\mu$ m<sup>2</sup> areas were imaged in each sample followed by three  $10 \times 10$   $\mu$ m<sup>2</sup> zoomed-in regions in the same respective areas.

**2.9. OECT Characterization.** OECT measurements (output and transfer curves) were obtained in aqueous NaCl (0.1 M) at room temperature using a pair of Keithley 2401 source-measure units to apply the source-drain voltage  $V_{DS}$  and gate voltage  $V_G$ .  $I$ - $V$  curves were also obtained using these source-measure units for dry pristine films drop-casted on IDMEs. The potential across the film was swept from  $-0.8$  to  $+0.8$  V while measuring the current. The line of best fit was calculated, and from the slope of this line, the resistance  $R$  was then calculated using Ohm's law. From the resistance  $R$ , the conductivity  $\sigma$  was calculated using the following equation:  $\sigma = L / (R \cdot W \cdot d)$  where  $L$ ,  $W$ , and  $d$  are the channel length, width, and thickness, respectively.<sup>35</sup> The threshold voltage  $V_{TH}$  was calculated from the output curves by plotting  $\sqrt{I_{DS}}$  versus  $V_G$  and extrapolating the linear portion of this curve to the *x*-axis.<sup>6,10</sup> The power consumption was calculated from the transfer curve data using the following equation:  $P = V_{DS} \cdot I_{DS} + V_G \cdot I_G$ , where  $I_G$  is the gate current.<sup>36</sup> Continuous stress testing was performed by recording the transient  $I_{DS}$  response to a square-wave  $V_G$  input oscillating between 0 and  $-0.6$  V with 90 s at each voltage. Intermittent stability was tested by recording the transfer curves of devices before and after 1, 3, 7, 14, and 21 days of immersion in aqueous NaCl (0.1 M). The electrochemical impedance spectra (Bode and Nyquist plots) were obtained using a potentiostat (Vertex, IVIUM) to apply various potentials with a sinusoidal voltage oscillation of  $\Delta V = 0.01$  V, at frequencies in the range of 10,000–0.1 Hz. From the EIS data, the capacitance as a function of frequency was extracted using the equation  $C = 1 / (2\pi f \text{Im}(Z))$ .<sup>17</sup> The capacitance of the film at  $+0.4$  V

was obtained at 0.1 Hz and this was divided by the full film area to give the volumetric capacitance,  $C^*$ .<sup>16</sup> The carrier mobility was then calculated from the volumetric capacitance and transconductance data. For these device measurements, three devices were characterized, and the results were reported as value  $\pm$  standard deviation unless otherwise specified.

### 3. RESULTS AND DISCUSSION

**3.1. Synthesis and Structural Characterization.** We synthesized the phosphonated EDOT derivative, EDOT-Phos, in three steps from the commercially available monomer, EDOT-OH, as shown in Scheme 1. The first two steps gave the desired products in high yields of 97.6 mol % for EDOT-Tos and 75.2 mol % for EDOT-I. We then synthesized EDOT-Phos by reacting EDOT-I with triisopropylphosphite ( $P(Oi-Pr)_3$ ). We periodically topped up the reaction mixture with aliquots of  $P(Oi-Pr)_3$  to maximize yield and counteract the effect of hydrolysis consuming the phosphite. Using this “top-up” method, we obtained EDOT-Phos in good yield (50.7 mol %) and high purity after column chromatography (Figures S7 to S13). We fully characterized all three monomers using solution NMR spectroscopy in  $CDCl_3$ . Table S1 summarizes the peak assignments from the one-dimensional NMR spectra. The one- and two-dimensional spectra of all monomers, including the decoupled  $^1H$  and  $^{31}P$  spectra and HSQC and HMBC spectra, are provided in the Supporting Information (Figures S1 to S13).

We synthesized the polymer PEDOT-Phos by chemical oxidative polymerization of EDOT-Phos with  $FeCl_3$  at room temperature (Scheme 1). This method was chosen for its mild reaction temperature and its reliability in synthesizing numerous CPs in the literature.<sup>37</sup> Treating the oxidized polymer with hydrazine monohydrate yielded the reduced polymer, PEDOT-Phos, which was soluble in dimethylsulfoxide (DMSO, 5.5 mg/mL) and chloroform ( $CHCl_3$ , 13.5 mg/mL). Solution  $^{31}P$ -NMR spectroscopy of PEDOT-Phos in  $CDCl_3$  (Figure 1A) revealed a symmetrical  $^{31}P$  singlet at 22.9 ppm, at almost the same chemical shift as the protected monomer (23.3 ppm, Figure S11), consistent with the

presence of the isopropyl-protected phosphonate group. We used gel permeation chromatography (GPC) of PEDOT-Phos in dimethylformamide (DMF) to obtain the number-average ( $\bar{M}_n = 78.8$  kDa) and weight-average molecular weights ( $\bar{M}_w = 158.6$  kDa) of the polymer. The measured value of  $\bar{M}_n$  corresponds to a polymer with 248 repeat units on average. The dispersity ( $\bar{M}_w/\bar{M}_n$ ) of PEDOT-Phos was 2.01, indicating a rather broad molecular mass distribution, but this result is typical for chemical oxidative syntheses of CPs including poly(3-alkylthiophenes)<sup>37</sup> and functionalized PEDOT derivatives.<sup>38</sup>

To probe the chemical structure of PEDOT-Phos, we performed ATR-FTIR and Raman spectroscopies. The ATR-FTIR transmission spectrum (Figure S14A) clearly showed the phosphonate  $P=O$  stretching mode as a strong, well-resolved peak at  $1258\text{ cm}^{-1}$ .<sup>39</sup> We also observed peaks at  $1079$  and  $1010\text{ cm}^{-1}$ , which may be assigned to  $C-O-C$  stretching and deformation of the ethylenedioxy ring<sup>40</sup> or to  $O-P-O$  and/or  $P-O-C$  stretching modes in the diisopropylphosphonate groups.<sup>39,41</sup> We acquired a Raman spectrum to obtain a clearer picture of the PEDOT backbone (Figure S14B). Here, the thiophene  $C=C$  and  $C-C$  stretching modes of PEDOT were clearly visible in the wavenumber range of  $1600\text{--}1300\text{ cm}^{-1}$ , as were for the aliphatic  $C-H$  stretching modes in the ethylenedioxy ring and the isopropyl protecting groups at  $3000\text{--}2800\text{ cm}^{-1}$ .<sup>40</sup> Table S2 provides an assignment of the observed bands in ATR-FTIR and Raman spectroscopies.

We performed XPS to further examine the polymer's chemical structure. The phosphonate environment appeared in the P 2p region as a spin-split doublet, with the P  $2p_{3/2}$  peak at a binding energy of 133.4 eV and the P  $2p_{1/2}$  peak at 134.3 eV (Figure 1B), similar to splitting patterns seen in a poly(fluorene) modified with diethylphosphonate ester groups.<sup>39</sup> Peak deconvolution in the S 2p region revealed a doublet with an S  $2p_{3/2}$  peak at a binding energy of 163.8 eV and the S  $2p_{1/2}$  peak at 165.0 eV (Figure 1C). The peaks in this doublet had an intensity ratio of 1:2 and an energy separation of 1.2 eV, which are consistent with thiophene sulfur atoms in the PEDOT backbone.<sup>42</sup> Peak deconvolution of the O 1s signal yielded two oxygen environments (Figure S14C). The primary environment had a binding energy of 532.6 eV for PEDOT-Phos and can be assigned to the ethylenedioxy oxygen atoms in PEDOT.<sup>42</sup> We also observed a second oxygen environment at a lower binding energy of 530.8 eV, which likely corresponded to oxygen atoms in phosphonate groups. However, the precise assignment of this peak is difficult, as Chan *et al.*<sup>43</sup> note for phosphonates in general. For example, the binding energy of  $P=O$  groups in phosphonated CPs is variously cited as being as low as 531.5 eV<sup>43</sup> or as high as 535 eV,<sup>44</sup> depending on the interactions of the phosphonate groups with other species. Finally, deconvolution in the C 1s region (Figure S14D) revealed two prominent environments. We assigned the main environment at 284.8 eV to carbon atoms in the thiophene rings and the isopropyl groups.<sup>42</sup> The second environment at 286.6 eV was attributed to  $C-O$  carbon atoms in the ethylenedioxy bridge<sup>42</sup> and the carbon atom in the  $C-P$  bond with the phosphonate group.<sup>45</sup> We also observed a small peak at 287.8 eV, which can be attributed to  $\pi-\pi^*$  shake-up processes in the PEDOT backbone.<sup>46</sup>

**3.2. Optical and Electrochemical Properties.** We performed UV-vis-NIR spectroscopy to characterize the optoelectronic properties of PEDOT-Phos solutions and films.

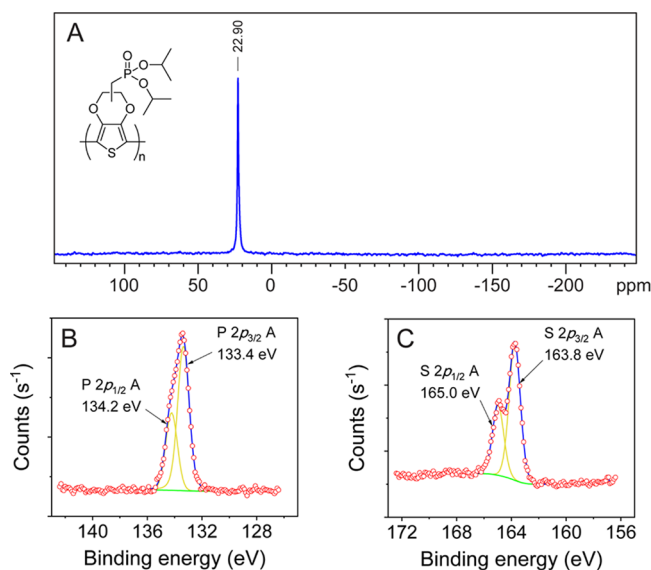


**Figure 1.** Structural characterization of PEDOT-Phos. (A)  $^{31}P$  solution NMR in  $CDCl_3$  showing the single phosphonate peak. (B) P 2p and (C) S 2p environments in the XPS spectrum of PEDOT-Phos.

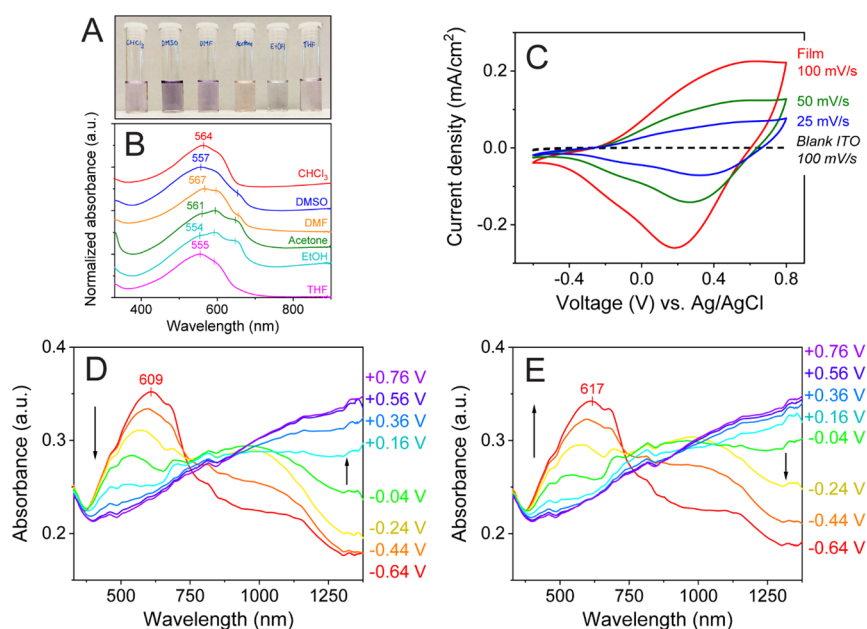


**Figure 2.** Optoelectronic properties of PEDOT-Phos solutions and films. (A) Photograph of PEDOT-Phos solutions in various solvents, from left to right:  $\text{CHCl}_3$ , DMSO, DMF, acetone, EtOH, and THF. The polymer was only sparingly soluble in acetone, EtOH, and THF. (B) UV-vis-NIR spectra of the solutions in (A). The absorbances were normalized to the range of [0, 1] and stacked vertically for clarity. (C) Cyclic voltammetry of PEDOT-Phos on ITO in NaCl (0.1 M in deionized water) at various scan rates over the potential range from  $-0.6$  to  $+0.8$  V. The film was first subjected to 20 relaxation cycles (scan rate of 100 mV/s and potential range from  $-0.6$  to  $+0.8$  V) to ensure a stable output. (D, E) *In situ* UV-vis-NIR spectroelectrochemistry of PEDOT-Phos/ITO films on ITO in NaCl (0.1 M in deionized water), with (D) increasing and (E) decreasing potential. The potentials were recorded vs Ag wire and are reported here relative to  $\text{Ag}/\text{AgCl} = \text{Ag wire} - 0.34$  V. Counter electrode: Pt wire.

In solution, PEDOT-Phos exhibited solvatochromism with a visible color change in various solvents as well as a shift in position of the  $\pi$ - $\pi^*$  transition band (Figure 2A,B). These changes correspond to changes in the effective conjugation length and optical band gap in solution, likely due to interactions between  $\pi$ -stacked polymer chains or possibly between the alkyl-protected phosphonate groups and solvent molecules as previously observed in phosphonated poly(fluorene)s.<sup>47</sup> There were also red-shifted vibronic shoulders in many of the solvents, which indicated the presence of  $\pi$ -stacked polymer chains with improved ordering in solution.<sup>48</sup> As for films of PEDOT-Phos, a pristine film exhibited a  $\pi$ - $\pi^*$  absorption peak at 544 nm, and vibronic shoulders were also visible at 488, 573, and 626 nm (Figure S15A), indicating the presence of some short-range ordering in  $\pi$ -stacked polymer chains in the solid state. The weak absorption peak at 988 nm may indicate the presence of residual polaronic charge carriers in the PEDOT backbone.<sup>49</sup> From this spectrum, a Tauc plot was constructed (Figure S15B), and the optical band gap energy was determined to be  $E_{g,\text{opt}} = 1.80$  eV, similar in value to other PEDOT derivatives.<sup>50,51</sup> Using DFT, we calculated the theoretical, direct electrical band gap to be 0.79 eV for both a  $\pi$ -stacked PEDOT-Phos crystal and an isolated PEDOT-Phos chain in a vacuum (Table S3 and Figure S17). This theoretical band gap energy is close to half the experimental value, which was also the case for previous DFT analysis of unsubstituted PEDOT.<sup>33</sup> Compared to the isolated chain, the PEDOT-Phos crystal also exhibited sub-band splitting close to the Fermi level (Figure S17B), which resulted from interchain interactions between the stacked polymer chains.<sup>33</sup> We also performed photoluminescence spectroscopy of PEDOT-Phos films to examine the polymer's emissive properties. The polymer exhibited a broad emission spectrum, with a maximum at a wavelength of 538 nm surrounded by several

smaller peaks (Figure S15C). These peaks corresponded to the zero-vibronic transition at 523 nm and vibronic states at longer wavelengths, as observed for other CPs including poly(*p*-phenylene vinylene)<sup>52</sup> and derivatives of poly(thiophene).<sup>53</sup>

Cyclic voltammetry (CV) of films of PEDOT-Phos on ITO revealed the polymer's reversible electrochemical activity in both aqueous and organic electrolytes (Figure 2C and Figure S18A, respectively). Here, current densities increased roughly proportional to the scan rate, indicating that the process was limited by the transport of charge carriers and not ions.<sup>16</sup> The shape of the voltammograms deviated from the box-like shape of a capacitive material, as observed in other PEDOT derivatives bearing carboxylate<sup>51</sup> and sulfonate<sup>23</sup> groups, with anodic and cathodic waves indicating that PEDOT-Phos underwent reversible oxidation and reduction in aqueous NaCl.<sup>54</sup> The onset of oxidation in this electrolyte was also low, at  $E_{\text{ox}} = -0.157$  V vs  $\text{Ag}/\text{AgCl}$  (Figure S18B). This value is comparable to that of other high-performance CPs used in OECTs, including the top-performing glycolated poly(thiophene) derivative p(g2T-TT) with  $E_{\text{ox}} = -0.14$  V.<sup>55</sup> The low oxidation onset of PEDOT-Phos is also encouraging for biological applications where the material must become electroactive at mild potentials to maintain cell viability.<sup>6</sup> From  $E_{\text{ox}}$  and  $E_{g,\text{opt}}$ , we estimated the energies of the highest occupied ( $E_{\text{HOMO}} = -4.74$  eV) and lowest unoccupied ( $E_{\text{LUMO}} = -2.95$  eV) orbitals as well as the ionization potential (IP = 4.74 eV). Likewise, DFT calculations yielded a theoretical IP of 4.66 eV for an isolated PEDOT-Phos chain, which was even lower than the experimental value in this idealized case (Table S3). We also calculated the effective masses of holes at the valence band edge ( $m_h^*/m_0^* = 0.111$ ) and electrons at the conduction band edge ( $m_e^*/m_0^* = 0.121$ ), relative to the free-electron mass at rest ( $m_0$ ) (Figure S17C). These values agreed

closely with the corresponding values for an isolated chain of unsubstituted PEDOT ( $m_h^*/m_0 = 0.093$ ;  $m_e^*/m_0 = 0.099$ ).<sup>33</sup>

We then performed *in situ* UV-vis-NIR spectroelectrochemistry of PEDOT-Phos/ITO films in aqueous NaCl (0.1 M) to observe the changes in optical properties during electrochemical switching. As the applied potential increased, the  $\pi$ - $\pi^*$  transition band at 609 nm rapidly decreased in intensity and a polaron band developed at 980 nm (Figure 2D). The polaron band was fully developed at  $-0.04$  V vs Ag/AgCl, representing milder conditions compared to p(g2T-TT), which required  $+0.40$  V vs Ag/AgCl for the polaron band to become fully visible.<sup>17</sup> At higher potentials ( $+0.16$  V vs Ag/AgCl and above), the polaron band began to disappear and a broad band appeared beyond 1600 nm, revealing the formation of bipolarons.<sup>9</sup> The diminishing  $\pi$ - $\pi^*$  band also became progressively blue-shifted as the potential increased, indicating the generation of charge carriers disrupting the backbone conjugation. Upon reversing the polarity, the bipolaron tail disappeared and the  $\pi$ - $\pi^*$  band was restored (Figure 2E), demonstrating the reversible electrochemistry of PEDOT-Phos, with only a slight red shift to 617 nm possibly reflecting changes in film morphology during cycling. We further demonstrated the reversibility and stability of switching in NaCl using *in situ* spectrochronoamperometry, as PEDOT-Phos films retained up to 94% of their original optical contrast after 20 min of continuous cycling between oxidizing and reducing potentials (Figure S18E). We also observed the reversible spectroelectrochemical behavior of PEDOT-Phos/ITO films in the organic electrolyte TBABF<sub>4</sub>/CH<sub>3</sub>CN (Figure S18C,D), demonstrating the electrochemical activity of PEDOT-Phos in both organic and aqueous environments.

We also used AFM to examine the morphology of PEDOT-Phos films before and after 20 and 100 cycles of CV in aqueous NaCl (0.1 M). The film morphology is shown in Figure S19 for a scan area of  $50 \times 50 \mu\text{m}$ , with both 2D micrographs and the corresponding vertical height profiles. The pristine film was non-uniform (Figure S19A), but the morphology changed drastically after electrochemical cycling, as evidenced by the greater periodicity of the height profiles and the polymer forming an open, honeycomb-like structure, with an interconnected network of polymer ridges surrounding pores (Figure S19B). The micrographs demonstrated the stability of this porous morphology after 100 cycles of CV (Figure S19C). Likewise, the film morphologies remained relatively unchanged when submerged in PBS (Figure S20). These results demonstrate that the porous morphology was promoted by electrochemical cycling. We postulate that during cycling, hydrated counterions are incorporated into the film and may accumulate around the polar phosphonate side groups of PEDOT-Phos.<sup>10,56</sup> These hydrated counterions push the polymer chains apart and disrupt the polymer clusters, forming the open, honeycomb morphology. The increased surface area in this morphology would allow additional ions to readily penetrate and interact with the polymer, greatly enhancing its volumetric capacitance and electrochemical response in aqueous OECTs as will be discussed next.<sup>21,57</sup>

**3.3. Performance in Organic Electrochemical Transistors.** Given the spectroelectrochemical response and morphological changes of PEDOT-Phos in aqueous media, we prepared films of PEDOT-Phos on IDMEs and utilized them in accumulation mode as OECTs operating in aqueous media. We first examined the  $I$ - $V$  characteristics and electrical resistance of pristine films prepared by drop-casting from

CHCl<sub>3</sub> onto IDMEs. The films showed linear  $I$ - $V$  curves (Figure 3A) with an average electrical resistance of  $11 \pm 3$  k $\Omega$ .

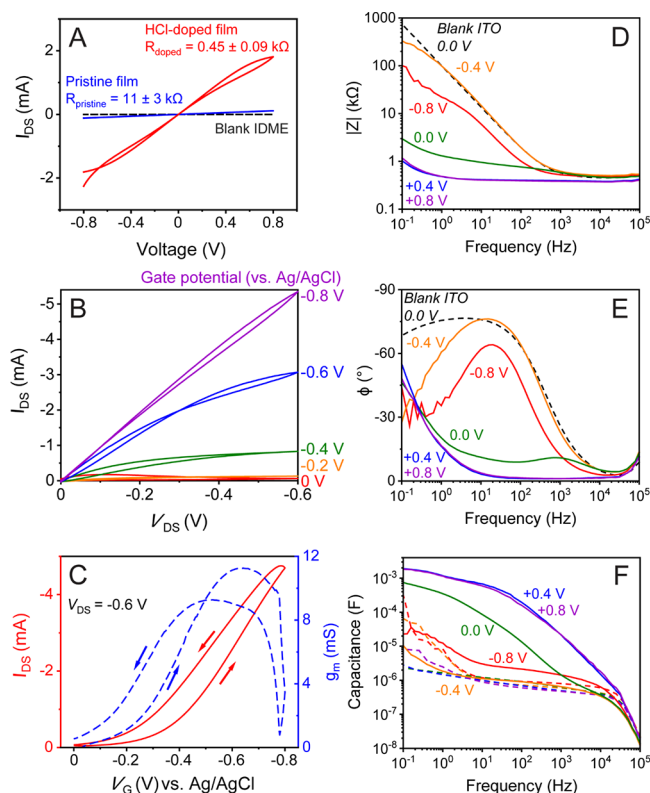


**Figure 3.** OECT characterization of PEDOT-Phos. (A)  $I$ - $V$  curves of a representative PEDOT-Phos film on an IDME before and after treatment with HCl. The resistances are shown on the figure and correspond to electrical conductivities of  $0.035 \pm 0.008$  mS cm<sup>-1</sup> (pristine film) and  $0.79 \pm 0.17$  mS cm<sup>-1</sup> (HCl-treated film). (B, C) OECT and electrochemical characterizations of a representative PEDOT-Phos device in aqueous NaCl (0.1 M): (B) Output curves for  $-0.8$  V  $\leq V_G \leq 0$  V and  $-0.6$  V  $\leq V_{DS} \leq 0$  V. (C) Transfer curve with transconductance for  $-0.8$  V  $\leq V_G \leq 0$  V with  $V_{DS} = -0.6$  V. (D-F) EIS characterization of this device at various applied potentials: (D) Bode impedance plots, (E) phase plots, and (F) capacitance as a function of frequency.

We then chemically doped these films with a non-oxidizing Brønsted acid, hydrochloric acid (HCl, 5  $\mu\text{L}$  dropped on the film surface). After acid treatment, the resistance dropped significantly to  $0.45 \pm 0.09$  k $\Omega$ , demonstrating that PEDOT-Phos is readily proton-doped by HCl, as has also been observed in unsubstituted PEDOT.<sup>58</sup> We further confirmed this behavior with UV-vis-NIR spectroscopy of PEDOT-Phos films before and after treatment with HCl (Figure S15A). Upon acid treatment, polaron and bipolaron bands became prominent, and the  $\pi$ - $\pi^*$  band decreased in intensity and was also slightly blue-shifted from 544 to 540 nm since the charge carriers lowered the polymer's conjugation length.

We characterized the output and transfer curves of PEDOT-Phos OECTs operated in aqueous NaCl (0.1 M) as shown in Figure 3B,C. The output curves revealed that the source-drain current ( $I_{DS}$ ) response was negligible at zero gate voltage and greatly increased in magnitude as  $V_G$  became more negative (Figure 3B). This response is consistent with the accumulation mode OECT operation, where a  $V_G$  must be applied to turn the device "ON". The transfer curves at  $V_{DS} = -0.6$  V again

showed the OECTs switching from OFF to ON when a non-zero  $V_G$  was applied (Figure 3C). We calculated from the transfer curve data the threshold voltage,  $V_{TH} = -0.161 \pm 0.005$  V (Figure S21A). This  $V_{TH}$  is close to 0 V, which indicates that little electrical input is required to switch the device “ON”, demonstrating the energy-efficient operation of our PEDOT-Phos-based OECTs. In fact, the low  $V_{TH}$  of PEDOT-Phos approaches that of the top-performing glycolated polymer, p(g2T-TT), in the same electrolyte ( $V_{TH} = -0.09$  V).<sup>10</sup> In contrast, water-stable, accumulation mode OECTs made from PEDOT-S capped with dioctylammonium and blended with poly(hexylthiophene sulfonic acid) (PTHS) exhibited transfer curves with a larger  $V_{TH}$  of around  $-0.4$  V, indicating their less efficient operation.<sup>59</sup> In another study, PTHS was capped with tetrabutylammonium to give water-stable OECTs, but these devices similarly exhibited a large  $V_{TH}$  of  $-0.5$  V.<sup>6</sup> Smaller  $V_{TH}$  values of  $-0.15$  to  $-0.20$  V were only achieved by copolymerization with hexylthiophene, necessitating more complex chemical synthesis, unlike our PEDOT-Phos with similar  $V_{TH}$  and straightforward polymerization by chemical oxidation. The low threshold voltage of PEDOT-Phos is especially promising for bioelectronics since it allows this polymer to be interfaced with cells without damaging them.<sup>6</sup>

From the transfer curves, we also calculated and plotted the transconductance,  $g_m$  (Figure 3C). As  $V_G$  became more negative, the transconductance reached a maximum value of  $9.3 \pm 1.8$  mS, with a power consumption of  $0.87 \pm 0.12$  mW (Figure S21C), which was lower than PEDOT:PSS OECTs with a similar  $g_m$  in the same electrolyte.<sup>60</sup> We then obtained transfer curves over an extended  $V_G$  range of  $+0.8$  to  $-0.8$  V (Figure S21B). From these, we compared the currents at gate voltages of  $-0.8$  V (ON) and  $+0.4$  V (OFF) and calculated the ON/OFF current ratio of this accumulation mode OECT to be  $I_{ON}/I_{OFF} = 618 \pm 54$ . This value is similar to those of existing PEDOT-based systems, including pristine PEDOT:PSS ( $I_{ON}/I_{OFF} = 541$ )<sup>24</sup> as well as PEDOT-S ( $I_{ON}/I_{OFF} = 650 \pm 210$ ) and its various CP blends.<sup>22</sup> Continuous electrochemical stress-testing revealed that PEDOT-Phos OECTs exhibit comparable electrochemical stability to other aqueous PEDOT-based OECTs (Figure S21D).<sup>61,62</sup> The PEDOT-Phos devices also showed excellent stability during long-term immersion in aqueous NaCl, with only a 5% decrease in the maximum  $I_{DS}$  in the transfer curves after 21 days of immersion (Figure S21E), which is promising for their potential application in stable, implantable devices in the human body. Although the switching speed of the drop-casted PEDOT-Phos devices (Figure S21D) was limited by the polymer's low mobility, similar results were shown for PEDOT:PSS devices when first developed,<sup>63</sup> where through optimizing, the device geometry response times were improved from several seconds to sub-millisecond timescales.<sup>9</sup>

After obtaining OECT measurements, we performed electrochemical impedance spectroscopy (EIS) of the films in aqueous NaCl at several potentials to obtain additional information on the device performances. As the applied potential increased from  $-0.8$  to  $+0.8$  V, the film's impedance in the low-frequency regime greatly decreased as the film was oxidized and charge carriers were generated (Figure 3D). The phase shift at intermediate frequencies ( $f = 10^1$ – $10^3$  Hz) also decreased in magnitude and approached  $0^\circ$  upon oxidation (Figure 3E), indicating a shift from capacitive to resistive character.<sup>17</sup> The Nyquist plots (Figure S21F) exhibited two

regimes. At high frequencies, the plot formed a semicircle with radius proportional to the resistance to charge transfer, while at low frequencies, we observed a sloped line at a  $45^\circ$  angle, indicative of a Warburg, mixed capacitance–impedance response, dominated by ionic diffusion between the film and electrolyte.<sup>64</sup> The two regimes were most clearly seen at 0 V, whereas at higher potentials, the radius of the semicircle became very small (inset of Figure S21F), indicating a greatly decreased resistance to charge transfer as the film was oxidized. We also computed and plotted the capacitance as a function of frequency (Figure 3F). The capacitance increased at more oxidizing potentials as the polymer increased in internal surface area to accommodate counterions into its volume. The capacitance behavior changed little above  $+0.4$  V since the polymer was fully oxidized. We extracted the capacitance at 0.1 Hz for the polymer at  $+0.4$  V and divided by the film volume to obtain the volumetric capacitance of PEDOT-Phos,  $C^* = 282 \pm 62$  F cm<sup>-3</sup> (Table S4). This capacitance greatly exceeds that of PEDOT:PSS treated with ethylene glycol ( $C^* = 39 \pm 3$  F cm<sup>-3</sup>), a common PEDOT-based system used in OECTs.<sup>65</sup> The capacitance of PEDOT-Phos is also similar to or exceeds those of many other CPs used in accumulation mode OECTs, including p(g2T-TT) with  $C^* = 241 \pm 94$  F cm<sup>-3</sup>.<sup>11,15,17</sup> The high transconductance and volumetric capacitance of PEDOT-Phos despite its hydrophobicity likely resulted from the nanoporous morphology produced during electrochemical cycling, which we observed with AFM in our morphological characterization (Figures S19 and S20). Recently, Huang *et al.*<sup>57</sup> also utilized nanoporous film morphologies to greatly enhance the transconductance and capacitance of hydrophobic polymers in aqueous OECTs. Kim *et al.*<sup>21</sup> likewise demonstrated that increasing both the crystallinity and nanoporosity of PEDOT:PSS films *via* treatment with sulfuric acid enhanced the volumetric capacitance of this polymer, up to  $C^* = 113$  F cm<sup>-3</sup>. The even higher  $C^*$  of our untreated, nanoporous PEDOT-Phos represents one of the highest volumetric capacitances achieved for a stand-alone, PEDOT-based conjugated polymer.

One limitation of the high  $C^*$  and nanoporous structure of PEDOT-Phos at present is the corresponding lower charge carrier mobility (Table S4). The incorporation of ions and water molecules during doping and the bulky pendant phosphonate groups close to the conjugated backbone would increase the spacing between  $\pi$ -stacked polymer chains as well as the overall microstructural disorder, lowering the interchain mobility of charge carriers.<sup>10,11</sup> We observed this effect in DFT simulations of crystalline PEDOT-Phos (Figure S16B), as the bulky protected groups led to a large  $\pi$ -stacking distance of 4.8 Å, compared to 3.4 Å for unsubstituted PEDOT.<sup>66</sup> As such, future developments in the molecular design of phosphonated PEDOT should account for the steric hindrance of pendant functionalities to optimize both capacitance and carrier mobility. Nonetheless, without any additives, post-treatment, or cross-linking, our PEDOT-Phos devices exhibited good transconductances; energy-efficient, accumulation mode operation with low threshold voltages; and excellent volumetric capacitance in a biocompatible, aqueous medium. These results together highlight the suitability of PEDOT-Phos as a stand-alone channel material in OECTs for monitoring or enhancing signal transduction in biological systems such as the human body.

## 4. CONCLUSIONS

We have synthesized and characterized PEDOT-Phos, an organic-processable derivative of PEDOT functionalized with isopropyl-protected, phosphonate pendant groups, and demonstrated its use as a stand-alone channel material in aqueous OECTs. PEDOT-Phos films exhibit reversible electrochemistry in a biocompatible, aqueous medium, with a low OECT threshold voltage ( $-0.161 \pm 0.005$  V) and a mild oxidation onset potential ( $-0.157$  V vs Ag/AgCl) comparable to high-performance, glycolated CPs. The nanoporous morphology of PEDOT-Phos affords it a high volumetric capacitance ( $282 \pm 62$  F cm<sup>-3</sup>), and OECTs based on PEDOT-Phos display efficient amplification in aqueous environments with accumulation mode operation, long-term stability when immersed in aqueous media, good transconductances ( $9.3 \pm 1.8$  mS), and ON/OFF ratios ( $618 \pm 54$ ) similar to other PEDOT-based systems. These results together demonstrate the suitability of PEDOT-Phos for bioelectronic applications requiring mild conditions for interfacing with cells.

To further improve the performance of phosphonated CPs including PEDOT-Phos in OECTs, we can utilize their synthetic flexibility to redesign their chemical structure and fine-tune their properties. We could improve charge carrier mobility and polymer packing by separating the phosphonate groups from the PEDOT backbone with a longer alkyl spacer, lowering the steric hindrance near the conjugated backbone. This change would enable closer, crystalline  $\pi$ -stacking and improve charge carrier mobility, which in turn would also improve the electrical conductivity and OECT switching speed.<sup>9</sup> It may also improve the accessibility of the phosphonate groups to other species, facilitating their interaction with analytes in biosensors or their coordination to metal substrates as electron injection layers in organic electronic devices.<sup>26</sup> We could also reduce the steric hindrance by deprotecting the phosphonate groups on PEDOT-Phos and so removing the bulky isopropyl groups. This measure would result in a water-processible, conjugated polyelectrolyte that may exhibit pH-dependent ionization and hence tailorable optical properties and polymer conformation in solution.<sup>44</sup> In OECTs, the deprotected phosphonate groups may also interact better with an aqueous electrolyte and improve ion mobility through the film, although the polymer's water solubility would necessitate cross-linking in this case. Furthermore, the low oxidation onset and IP of PEDOT-Phos demonstrate the benefits of utilizing electron-rich moieties, such as the ethylenedioxy bridges in PEDOT, as a design strategy for CPs to facilitate electrochemical switching and device operation under mild conditions, a requirement for bioelectronic applications. The ON/OFF ratio of PEDOT-Phos, while presently similar to that of PEDOT:PSS, could also be further improved by fabricating thinner films with greater permeability to ions or by optimizing the construction of the layered device.<sup>67,68</sup> PEDOT-Phos, therefore, is not only a promising material for aqueous, accumulation mode OECTs, as we have demonstrated, it is also the first of a series of phosphonated PEDOT derivatives whose tailored chemistries should have excellent potential for organic bioelectronics.

## ■ ASSOCIATED CONTENT

### SI Supporting Information

The Supporting Information is available free of charge at <https://pubs.acs.org/doi/10.1021/acs.chemmater.1c02936>.

NMR spectra of monomers and polymers; ATR-FTIR and Raman spectra of PEDOT-Phos and peak assignments; XPS, UV-vis-NIR, and PL spectra of PEDOT-Phos; DFT-calculated molecular geometries, band structures, and effective masses of charge carriers; CV and *in situ* spectroelectrochemistry in TBABF<sub>4</sub>/CH<sub>3</sub>CN; *in situ* spectrochronoamperometry in aqueous NaCl; AFM micrographs; threshold voltage, extended transfer curve, OECT stability, Nyquist plots, and summary of parameters for PEDOT-Phos OECTs (PDF)

## ■ AUTHOR INFORMATION

### Corresponding Author

**Damia Mawad** – School of Materials Science and Engineering, UNSW Sydney, Sydney, New South Wales 2052, Australia; Australian Centre for NanoMedicine, UNSW Sydney, Sydney, New South Wales 2052, Australia; [orcid.org/0000-0002-6965-3232](https://orcid.org/0000-0002-6965-3232); Email: [damia.mawad@unsw.edu.au](mailto:damia.mawad@unsw.edu.au)

### Authors

**Jonathan Hopkins** – School of Materials Science and Engineering, UNSW Sydney, Sydney, New South Wales 2052, Australia

**Kristina Fidanovski** – School of Materials Science and Engineering, UNSW Sydney, Sydney, New South Wales 2052, Australia

**Lorenzo Travaglini** – School of Materials Science and Engineering, UNSW Sydney, Sydney, New South Wales 2052, Australia

**Daniel Ta** – School of Science, Western Sydney University, Penrith, NSW 2751, Australia

**James Hook** – School of Chemistry, University of New South Wales, Sydney, NSW 2052, Australia

**Pawel Wagner** – Intelligent Polymer Research Institute and ARC Centre of Excellence for Electromaterials Science, University of Wollongong, Wollongong, New South Wales 2522, Australia; [orcid.org/0000-0003-1926-9862](https://orcid.org/0000-0003-1926-9862)

**Klaudia Wagner** – Intelligent Polymer Research Institute and ARC Centre of Excellence for Electromaterials Science, University of Wollongong, Wollongong, New South Wales 2522, Australia

**Antonio Lauto** – School of Science, Western Sydney University, Penrith, NSW 2751, Australia; [orcid.org/0000-0003-4593-5603](https://orcid.org/0000-0003-4593-5603)

**Claudio Cazorla** – Departament de Física, Universitat Politècnica de Catalunya, Barcelona 08034, Spain; [orcid.org/0000-0002-6501-4513](https://orcid.org/0000-0002-6501-4513)

**David Officer** – Intelligent Polymer Research Institute and ARC Centre of Excellence for Electromaterials Science, University of Wollongong, Wollongong, New South Wales 2522, Australia; [orcid.org/0000-0001-5465-9781](https://orcid.org/0000-0001-5465-9781)

Complete contact information is available at:

<https://pubs.acs.org/doi/10.1021/acs.chemmater.1c02936>

### Author Contributions

The manuscript was written through contributions from all authors. All authors have given approval to the final version of the manuscript.

### Notes

The authors declare no competing financial interest.

## ACKNOWLEDGMENTS

D.M., D.O., and A.L. would like to acknowledge the Australian Research Council, Discovery Project Grant DP190102560, for funding this research. The authors would like to acknowledge the use of facilities and the assistance of Dr. Anne Rich of the Spectroscopy Laboratory, Dr. Bill Bin Gong and Dr. Yu Wang in the Solid State & Elemental Analysis Unit, as well as the members of the NMR Facility under the Mark Wainwright Analytical Centre at UNSW Sydney. The authors also gratefully acknowledge the use of facilities at the Australian National Fabrication Facility at the University of Wollongong for GPC measurements.

## REFERENCES

- (1) Rivnay, J.; Inal, S.; Salleo, A.; Owens, R. M.; Berggren, M.; Malliaras, G. G. Organic Electrochemical Transistors. *Nat. Rev. Mater.* **2018**, *3*, 17086.
- (2) Liao, J.; Si, H.; Zhang, X.; Lin, S. Functional Sensing Interfaces of PEDOT:PSS Organic Electrochemical Transistors for Chemical and Biological Sensors: A Mini Review. *Sensors* **2019**, *19*, 218.
- (3) Bai, L.; Elósegui, C. G.; Li, W.; Yu, P.; Fei, J.; Mao, L. Biological Applications of Organic Electrochemical Transistors: Electrochemical Biosensors and Electrophysiology Recording. *Front. Chem.* **2019**, *7*, 313.
- (4) Wang, N.; Yang, A.; Fu, Y.; Li, Y.; Yan, F. Functionalized Organic Thin Film Transistors for Biosensing. *Acc. Chem. Res.* **2019**, *52*, 277–287.
- (5) Rivnay, J.; Leleux, P.; Ferro, M.; Sessolo, M.; Williamson, A.; Koutsouras, D. A.; Khodagholy, D.; Ramuz, M.; Strakosas, X.; Owens, R. M.; Benar, C.; Badier, J.-M.; Bernard, C.; Malliaras, G. G. High-Performance Transistors for Bioelectronics through Tuning of Channel Thickness. *Sci. Adv.* **2015**, *1*, No. e1400251.
- (6) Schmode, P.; Ohayon, D.; Reichstein, P. M.; Savva, A.; Inal, S.; Thelakkat, M. High-Performance Organic Electrochemical Transistors Based on Conjugated Polyelectrolyte Copolymers. *Chem. Mater.* **2019**, *31*, 5286–5295.
- (7) Inal, S.; Malliaras, G. G.; Rivnay, J. Benchmarking Organic Mixed Conductors for Transistors. *Nat. Commun.* **2017**, *8*, 1767.
- (8) Li, P.; Lei, T. Molecular Design Strategies for High-performance Organic Electrochemical Transistors. *J. Polym. Sci.* **2021**, 1–16.
- (9) Moser, M.; Ponder, J. F., Jr.; Wadsworth, A.; Giovannitti, A.; McCulloch, I. Materials in Organic Electrochemical Transistors for Bioelectronic Applications: Past, Present, and Future. *Adv. Funct. Mater.* **2019**, *29*, 1807033–1807015.
- (10) Savva, A.; Cendra, C.; Giugni, A.; Torre, B.; Surgailis, J.; Ohayon, D.; Giovannitti, A.; McCulloch, I.; Di Fabrizio, E.; Salleo, A.; Rivnay, J.; Inal, S. Influence of Water on the Performance of Organic Electrochemical Transistors. *Chem. Mater.* **2019**, *31*, 927–937.
- (11) Savagian, L. R.; Österholm, A. M.; Ponder, J. F., Jr.; Barth, K. J.; Rivnay, J.; Reynolds, J. R. Balancing Charge Storage and Mobility in an Oligo(Ether) Functionalized Dioxathiophene Copolymer for Organic- and Aqueous- Based Electrochemical Devices and Transistors. *Adv. Mater.* **2018**, *30*, 1804647–1804646.
- (12) Hopkins, J.; Fidanovski, K.; Lauto, A.; Mawad, D. All-Organic Semiconductors for Electrochemical Biosensors: An Overview of Recent Progress in Material Design. *Front. Bioeng. Biotechnol.* **2019**, *7*, 1–8.
- (13) Inal, S.; Rivnay, J.; Sui, A. O.; Malliaras, G. G.; McCulloch, I. Conjugated Polymers in Bioelectronics. *Acc. Chem. Res.* **2018**, *51*, 1368–1376.
- (14) Hopkins, J.; Travaglini, L.; Lauto, A.; Cramer, T.; Fraboni, B.; Seidel, J.; Mawad, D. Photoactive Organic Substrates for Cell Stimulation: Progress and Perspectives. *Adv. Mater. Technol.* **2019**, *4*, 1800744.
- (15) Inal, S.; Rivnay, J.; Leleux, P.; Ferro, M.; Ramuz, M.; Brendel, J. C.; Schmidt, M. M.; Thelakkat, M.; Malliaras, G. G. A High Transconductance Accumulation Mode Electrochemical Transistor. *Adv. Mater.* **2014**, *26*, 7450–7455.
- (16) Khau, B. V.; Savagian, L. R.; De Keersmaecker, M.; Gonzalez, M. A.; Reichmanis, E. Carboxylic Acid Functionalization Yields Solvent-Resistant Organic Electrochemical Transistors. *ACS Mater. Lett.* **2019**, *1*, 599–605.
- (17) Giovannitti, A.; Sbircea, D.-T.; Inal, S.; Nielsen, C. B.; Bandiello, E.; Hanifi, D. A.; Sessolo, M.; Malliaras, G. G.; McCulloch, I.; Rivnay, J. Controlling the Mode of Operation of Organic Transistors through Side-Chain Engineering. *Proc. Natl. Acad. Sci. U. S. A.* **2016**, *113*, 12017–12022.
- (18) Groenendaal, L.; Jonas, F.; Freitag, D.; Pielartzik, H.; Reynolds, J. R. Poly(3,4-Ethylenedioxythiophene) and Its Derivatives: Past, Present, and Future. *Adv. Mater.* **2000**, *12*, 481–494.
- (19) Hu, D.; Zhang, L.; Zhang, K.; Duan, X.; Xu, J.; Dong, L.; Sun, H.; Zhu, X.; Zhen, S. Synthesis and Characterization of PEDOT Derivative with Carboxyl Group and Its Chemo Sensing Application as Enhanced Optical Materials. *J. Appl. Polym. Sci.* **2015**, *132*, 1–9.
- (20) Khodagholy, D.; Rivnay, J.; Sessolo, M.; Gurfinkel, M.; Leleux, P.; Jimison, L. H.; Stavrinidou, E.; Herve, T.; Sanaur, S.; Owens, R. M.; Malliaras, G. G. High Transconductance Organic Electrochemical Transistors. *Nat. Commun.* **2013**, *4*, 2133.
- (21) Kim, S.-M.; Kim, C.-H.; Kim, Y.; Kim, N.; Lee, W.-J.; Lee, E.-H.; Kim, D.; Park, S.; Lee, K.; Rivnay, J.; Yoon, M.-H. Influence of PEDOT:PSS Crystallinity and Composition on Electrochemical Transistor Performance and Long-Term Stability. *Nat. Commun.* **2018**, *9*, 3858.
- (22) Zeglio, E.; Vagin, M.; Musumeci, C.; Ajjan, F. N.; Gabrielsson, R.; Trinh, X. T.; Son, N. T.; Maziz, A.; Solin, N.; Inganäs, O. Conjugated Polyelectrolyte Blends for Electrochromic and Electrochemical Transistor Devices. *Chem. Mater.* **2015**, *27*, 6385–6393.
- (23) Beaumont, C.; Turgeon, J.; Idir, M.; Neusser, D.; Lapointe, R.; Caron, S.; Dupont, W.; D'Astous, D.; Shamsuddin, S.; Hamza, S.; Landry, É.; Ludwigs, S.; Leclerc, M. Water-Processable Self-Doped Conducting Polymers via Direct (Hetero)Arylation Polymerization. *Macromolecules* **2021**, *54*, 5464–5472.
- (24) Fan, J.; Rezaie, S. S.; Facchini-Rakovich, M.; Gudi, D.; Montemagno, C.; Gupta, M. Tuning PEDOT:PSS Conductivity to Obtain Complementary Organic Electrochemical Transistor. *Org. Electron.* **2019**, *66*, 148–155.
- (25) Kafarski, P. Phosphonates: Their Natural Occurrence and Physiological Role. In *Contemporary Topics about Phosphorus in Biology and Materials*; Churchill, D. G.; Sikirić, M. D.; Čolović, B.; Milhofer, H. F., Eds.; *IntechOpen: London*, 2020; pp. 95–113, DOI: 10.5772/intechopen.87155.
- (26) Wu, C.-S.; Chou, C.-Y.; Chen, Y. Copolyfluorenes Containing Partially Hydrolyzed Phosphonate Pendant Groups: Synthesis, Characterization and Application as Electron Injection Layers for Enhanced Electroluminescence of PLEDs. *J. Mater. Chem. C* **2014**, *2*, 6665–6674.
- (27) Guo, X.; Qin, C.; Cheng, Y.; Xie, Z.; Ceng, Y.; Jing, X.; Wang, F.; Wang, L. White Electroluminescence from a Phosphonate-Functionalized Single-Polymer System with Electron-Trapping Effect. *Adv. Mater.* **2009**, *21*, 3682–3688.
- (28) Pavlishchuk, V. V.; Addison, A. W. Conversion Constants for Redox Potentials Measured versus Different Reference Electrodes in Acetonitrile Solutions at 25°C. *Inorg. Chim. Acta* **2000**, *298*, 97–102.
- (29) Katana. UNSW: Sydney, 2010, 10.26190/669x-A286 (accessed October 5, 2021).
- (30) Kresse, G.; Furthmüller, J. Efficient Iterative Schemes for Ab Initio Total-Energy Calculations Using a Plane-Wave Basis Set. *Phys. Rev. B* **1996**, *54*, 11169–11186.
- (31) Perdew, J. P.; Burke, K.; Ernzerhof, M. Generalized Gradient Approximation Made Simple. *Phys. Rev. Lett.* **1996**, *77*, 3865–3868.
- (32) Grimme, S.; Antony, J.; Ehrlich, S.; Krieg, H. A Consistent and Accurate Ab Initio Parametrization of Density Functional Dispersion Correction (DFT-D) for the 94 Elements H-Pu. *J. Chem. Phys.* **2010**, *132*, 154104.

- (33) Kim, E. G.; Brédas, J. L. Electronic Evolution of Poly(3,4-Ethylenedioxythiophene) (PEDOT): From the Isolated Chain to the Pristine and Heavily Doped Crystals. *J. Am. Chem. Soc.* **2008**, *130*, 16880–16889.
- (34) Bagayoko, D. Understanding Density Functional Theory (DFT) and Completing It in Practice. *AIP Adv.* **2014**, *4*, 127104.
- (35) Travaglini, L.; Micolich, A. P.; Cazorla, C.; Zeglio, E.; Lauto, A.; Mawad, D. Single-Material OECT-Based Flexible Complementary Circuits Featuring Polyaniline in Both Conducting Channels. *Adv. Funct. Mater.* **2021**, *31*, 2007205–2007210.
- (36) Wang, X.; Meng, X.; Zhu, Y.; Ling, H.; Chen, Y.; Li, Z.; Hartel, M. C.; Dokmeci, M. R.; Zhang, S.; Khademhosseini, A. A Sub-1-V, Microwatt Power-Consumption Iontronic Pressure Sensor Based on Organic Electrochemical Transistors. *IEEE Electron Device Lett.* **2021**, *42*, 46–49.
- (37) McCullough, R. D. The Chemistry of Conducting Polythiophenes. *Adv. Mater.* **1998**, *10*, 93–116.
- (38) Yano, H.; Kudo, K.; Marumo, K.; Okuzaki, H. Fully Soluble Self-Doped Poly(3,4-Ethylenedioxythiophene) with an Electrical Conductivity Greater than 1000 S Cm<sup>-1</sup>. *Sci. Adv.* **2019**, *5*, eaav9492–eaav9410.
- (39) Xu, M.; Han, X.; Wang, T.; Li, S.; Hua, D. Conjugated Microporous Polymers Bearing Phosphonate Ligands as an Efficient Sorbent for Potential Uranium Extraction from High-Level Liquid Wastes. *J. Mater. Chem. A* **2018**, *6*, 13894–13900.
- (40) Garreau, S.; Louarn, G.; Buisson, J. P.; Froyer, G.; Lefrant, S. In Situ Spectroelectrochemical Raman Studies of Poly(3,4-Ethylenedioxythiophene) (PEDT). *Macromolecules* **1999**, *32*, 6807–6812.
- (41) Smirnova, I. N.; Cuisset, A.; Hindle, F.; Mouret, G.; Bocquet, R.; Piralí, O.; Roy, P. Gas-Phase Synchrotron FTIR Spectroscopy of Weakly Volatile Alkyl Phosphonate and Alkyl Phosphate Compounds: Vibrational and Conformational Analysis in the Terahertz/Far-IR Spectral Domain. *J. Phys. Chem. B* **2010**, *114*, 16936–16947.
- (42) Jönsson, S. K. M.; Birgeron, J.; Crispin, X.; Greczynski, G.; Osikowicz, W.; Denier van der Gon, A. W.; Salaneck, W. R.; Fahlman, M. The Effects of Solvents on the Morphology and Sheet Resistance in Poly(3,4-Ethylenedioxythiophene)-Polystyrenesulfonic Acid (PEDOT-PSS) Films. *Synth. Met.* **2003**, *139*, 1–10.
- (43) Chan, H. S. O.; Ho, P. K. H.; Ng, S. C.; Tan, B. T. G.; Tan, K. L. A New Water-Soluble, Self-Doping Conducting Polyaniline from Poly(o-Aminobenzylphosphonic Acid) and Its Sodium Salts: Synthesis and Characterization. *J. Am. Chem. Soc.* **1995**, *117*, 8517–8523.
- (44) Viinikanoja, A.; Lukkari, J.; Ääritalo, T.; Laiho, T.; Kankare, J. Phosphonic Acid Derivatized Polythiophene: A Building Block for Metal Phosphonate and Polyelectrolyte Multilayers. *Langmuir* **2003**, *19*, 2768–2775.
- (45) Adden, N.; Gamble, L. J.; Castner, D. G.; Hoffmann, A.; Gross, G.; Menzel, H. Phosphonic Acid Monolayers for Binding of Bioactive Molecules to Titanium Surfaces. *Langmuir* **2006**, *22*, 8197–8204.
- (46) Denier van der Gon, A. W.; Birgeron, J.; Fahlman, M.; Salaneck, W. R. Modification of PEDOT–PSS by Low-Energy Electrons. *Org. Electron.* **2002**, *3*, 111–118.
- (47) Zhou, G.; Qian, G.; Ma, L.; Cheng, Y.; Xie, Z.; Wang, L.; Jing, X.; Wang, F. Polyfluorenes with Phosphonate Groups in the Side Chains as Chemosensors and Electroluminescent Materials. *Macromolecules* **2005**, *38*, 5416–5424.
- (48) Murphy, A. R.; Liu, J.; Luscombe, C.; Kavulak, D.; Fréchet, J. M. J.; Kline, R. J.; McGehee, M. D. Synthesis, Characterization, and Field-Effect Transistor Performance of Carboxylate-Functionalized Polythiophenes with Increased Air Stability. *Chem. Mater.* **2005**, *17*, 4892–4899.
- (49) Domagala, W.; Pilawa, B.; Lapkowski, M. Quantitative In-Situ EPR Spectroelectrochemical Studies of Doping Processes in Poly(3,4-Alkylendioxythiophene)s. Part 1: PEDOT. *Electrochim. Acta* **2008**, *53*, 4580–4590.
- (50) Schottland, P.; Fichet, O.; Teyssié, D.; Chevrot, C. Langmuir-Blodgett Films of an Alkoxy Derivative of Poly(3,4-Ethylenedioxythiophene). *Synth. Met.* **1999**, *101*, 7–8.
- (51) Mawad, D.; Artzy-Schnirman, A.; Tonkin, J.; Ramos, J.; Inal, S.; Mahat, M. M.; Darwish, N.; Zwi-Dantsis, L.; Malliaras, G. G.; Gooding, J. J.; Lauto, A.; Stevens, M. M. Electroconductive Hydrogel Based on Functional Poly(Ethylenedioxy Thiophene). *Chem. Mater.* **2016**, *28*, 6080–6088.
- (52) Arkhipov, V. I.; Bäessler, H.; Deussen, M.; Göbel, E. O.; Kersting, R.; Kurz, H.; Lemmer, U.; Mahrt, R. F. Field-Induced Exciton Breaking in Conjugated Polymers. *Phys. Rev. B* **1995**, *52*, 4932–4940.
- (53) Alves, M. R. A.; Calado, H. D. R.; Donnici, C. L.; Matencio, T. Synthesis and Characterization of New 3-Substituted Thiophene Copolymers. *J. Braz. Chem. Soc.* **2011**, *22*, 248–256.
- (54) Moser, M.; Savagian, L. R.; Savva, A.; Matta, M.; Ponder, J. F., Jr.; Hidalgo, T. C.; Ohayon, D.; Hallani, R.; Reisjalali, M.; Troisi, A.; Wadsworth, A.; Reynolds, J. R.; Inal, S.; McCulloch, I. Ethylene Glycol-Based Side Chain Length Engineering in Polythiophenes and Its Impact on Organic Electrochemical Transistor Performance. *Chem. Mater.* **2020**, *32*, 6618–6628.
- (55) Hallani, R. K.; Paulsen, B. D.; Petty, A. J., II; Sheelamantula, R.; Moser, M.; Thorley, K. J.; Sohn, W.; Rashid, R. B.; Savva, A.; Moro, S.; Parker, J. P.; Drury, O.; Alsufyani, M.; Neophytou, M.; Kosco, J.; Inal, S.; Costantini, G.; Rivnay, J.; McCulloch, I. Regiochemistry-Driven Organic Electrochemical Transistor Performance Enhancement in Ethylene Glycol-Functionalized Polythiophenes. *J. Am. Chem. Soc.* **2021**, *143*, 11007–11018.
- (56) Cendra, C.; Giovannitti, A.; Savva, A.; Venkatraman, V.; McCulloch, I.; Salleo, A.; Inal, S.; Rivnay, J. Role of the Anion on the Transport and Structure of Organic Mixed Conductors. *Adv. Funct. Mater.* **2019**, *29*, 1807034.
- (57) Huang, L.; Wang, Z.; Chen, J.; Wang, B.; Chen, Y.; Huang, W.; Chi, L.; Marks, T. J.; Facchetti, A. Porous Semiconducting Polymers Enable High-Performance Electrochemical Transistors. *Adv. Mater.* **2021**, *33*, 2007041.
- (58) Howden, R. M.; McVay, E. D.; Gleason, K. K. OCVD Poly(3,4-Ethylenedioxythiophene) Conductivity and Lifetime Enhancement via Acid Rinse Dopant Exchange. *J. Mater. Chem. A* **2013**, *1*, 1334–1340.
- (59) Zeglio, E.; Schmidt, M. M.; Thelakkat, M.; Gabrielsson, R.; Solin, N.; Inganäs, O. Conjugated Polyelectrolyte Blends for Highly Stable Accumulation-Mode Electrochemical Transistors. *Chem. Mater.* **2017**, *29*, 4293–4300.
- (60) Koklu, A.; Wustoni, S.; Musteata, V. E.; Ohayon, D.; Moser, M.; McCulloch, I.; Nunes, S. P.; Inal, S. Microfluidic Integrated Organic Electrochemical Transistor with a Nanoporous Membrane for Amyloid- $\beta$  Detection. *ACS Nano* **2021**, *15*, 8130–8141.
- (61) Lingstedt, L. V.; Ghittorelli, M.; Lu, H.; Koutsouras, D. A.; Marszalek, T.; Torricelli, F.; Crăciun, N. I.; Gkoupidenis, P.; Blom, P. W. M. Effect of DMSO Solvent Treatments on the Performance of PEDOT:PSS Based Organic Electrochemical Transistors. *Adv. Electron. Mater.* **2019**, *5*, 1800804.
- (62) Zeglio, E.; Eriksson, J.; Gabrielsson, R.; Solin, N.; Inganäs, O. Highly Stable Conjugated Polyelectrolytes for Water-Based Hybrid Mode Electrochemical Transistors. *Adv. Mater.* **2017**, *29*, 1605787.
- (63) Havener, R.; Boyea, J.; Malone, E.; Bernards, D.; DeFranco, J.; Malliaras, G.; Lipson, H. Freeform Fabrication of Organic Electrochemical Transistors. In *International Solid Freeform Fabrication Symposium*; 2007, pp. 60–73.
- (64) Wustoni, S.; Savva, A.; Sun, R.; Bihar, E.; Inal, S. Enzyme-Free Detection of Glucose with a Hybrid Conductive Gel Electrode. *Adv. Mater. Interfaces* **2019**, *6*, 1800928.
- (65) Rivnay, J.; Inal, S.; Collins, B. A.; Sessolo, M.; Stavrinidou, E.; Strakosas, X.; Tassone, C.; Delongchamp, D. M.; Malliaras, G. G. Structural Control of Mixed Ionic and Electronic Transport in Conducting Polymers. *Nat. Commun.* **2016**, *7*, 1–9.
- (66) Aasmundtveit, K. E.; Samuelsen, E. J.; Pettersson, L. A. A.; Inganäs, O.; Johansson, T.; Feidenhans'l, R. Structure of Thin Films of Poly(3,4-Ethylenedioxythiophene). *Synth. Met.* **1999**, *101*, 561–564.

(67) Kumar, P.; Yi, Z.; Zhang, S.; Sekar, A.; Soavi, F.; Cicoira, F. Effect of Channel Thickness, Electrolyte Ions, and Dissolved Oxygen on the Performance of Organic Electrochemical Transistors. *Appl. Phys. Lett.* **2015**, *107*, No. 053303.

(68) Zhang, S.; Li, Y.; Tomasello, G.; Anthonisen, M.; Li, X.; Mazzeo, M.; Genco, A.; Grutter, P.; Cicoira, F. Tuning the Electromechanical Properties of PEDOT:PSS Films for Stretchable Transistors And Pressure Sensors. *Adv. Electron. Mater.* **2019**, *5*, 1900191–1900197.

**HAZARD AWARENESS  
REDUCES LAB INCIDENTS**

**ACS Essentials of  
Lab Safety for  
General Chemistry**

A new course from the  
American Chemical Society

ACS Institute  
Learn. Develop. Excel.

EXPLORE  
ORGANIZATIONAL  
SALES  
[solutions.acs.org/essentialsoflabsafety](https://solutions.acs.org/essentialsoflabsafety)

REGISTER FOR  
INDIVIDUAL ACCESS  
[institute.acs.org/courses/essentials-lab-safety.html](https://institute.acs.org/courses/essentials-lab-safety.html)